Comparison of the efficiency of chopped and non-rectangular electrical stimulus waveforms in activating small vagus nerve fibers

Mélissa Dali, Chloé Picq, Olivier Rossel, Pawel Maciejasz, Charles-Henri Malbert, David Guiraud

Highlights

- Non rectangular waveforms should be considered for long term vagus nerve stimulation.
- Stimulation of duodenal neurons can be more charge efficient using ramp or quarter sine waveforms instead of rectangular waveform.
- MRG (Mc.Intyre-Richardson-Grill) axon model is an appropriate candidate to study complex non-rectangular waveforms

Comparison of the efficiency of chopped and non-rectangular electrical stimulus waveforms in activating small vagus nerve fibers

Mélissa Dali[a], Chloé Picq[b], Olivier Rossel[c], Pawel Maciejasz[d], Charles-Henri Malbert[e], David Guiraud[a]

[a] *INRIA, University of Montpellier, Montpellier, France*
[b] *Axonic, Sophia Antipolis, France*
[c] *University hospital of Montpellier, Montpellier, France*
[d] *Otto Bock HealthCare GmbH, Duderstadt, Germany*
[e] *INRA, Rennes, France*

Abstract

Background. In the context of morbid obesity, vagus nerve stimulation could be used to control gastric function targeting the small afferent B-fibers and C-fibers. Compared to large A-fibers, activation thresholds of these small efferent fibers are 10 to 100 times greater, inducing technical constraints and possible nerve damages. Although rectangular waveform is commonly used in nerve stimulation, recent modeling and experimental studies suggest that non-rectangular waveforms could reduced the charge injected by the stimulator. **New method.** The objective of the present study is to evaluate the charge injection of complex waveforms such as the ramp, quarter sine and chopped pulses in the context of vagus nerve stimulation. We performed *in-vivo* study on the porcine abdominal vagus nerves and evaluated charge injection at activation thresholds. A modeling study was performed to further extent the results obtained *in-vivo*. **Comparison with existing method.** Compared to the rectangular pulse, the ramp and quarter sine waveforms activated gastric fibers with the lowest charge injection: -23.2% and -30.1% respectively. The efficacy of chopped pulses is questioned through the consideration of the strength-duration curve. **Conclusion.** Continuous ramp and quarter sine waveforms effectively activate small diameter fibers. These pulse shapes may be considered for long-term vagus nerve stimulation. The results predicted by computational models were qualitatively consistent with experiments. This suggested the relevance of using modeling in the context of complex waveforms prior to future *in-vivo* tests.

Keywords: Vagus nerve stimulation, obesity, neuromodulation, nerve modeling, burst waveforms, chopped pulses, compound action potential.

1. Introduction

Vagus nerve stimulation (VNS) is a well-established technique successfully used to treat intractable epilepsy [1, 2] and refractory depression [3, 4]. VNS is also a promising therapy in the treatment of cardiac disorders and morbid obesity [5, 6, 7, 8, 9]. However, contrary to most of VNS applications, weight reduction and/or insulin sensitivity improvement required the stimulation of both vagal trunks; a mandatory condition that cannot be achieved at the cervical level without significant cardiac side-effects some of which being life threatening [7]. As a consequence, most of the studies targeted obesity [10] have used bilateral stimulation after the cardiac branches e.g. at the diaphragmatic level. At this level, the control of the gastric function requires the activation of small afferent nerve fibers, i.e. type B or C [11]. Thresholds for activation of B-fibers and C-fibers are respectively 2–3 and 10–100 times greater than the threshold of the large A-fibers (Aα, Aβ, Aγ) [12]. Membrane depolarization requires significant electrical charge injection on a fragile tissue over long periods, that may cause damages at the electrode-tissue interface level [13]. Therefore, charge reduction is mandatory. Optimizing the pulse shape (waveform) while reducing charge needed to activate small axons can reduce constraints on stimulator and preserve the tissues. Previous studies suggested that non-rectangular waveforms could activate fibers of the peripheral nervous system with less charge than rectangular ones: i) using ramp, exponential, gaussian but continuous waveforms [14, 15], ii) chopped waveforms [16, 17, 18] also named burst-modulated waveforms. Chopped waveforms seem promising especially for B and C fibers as it was shown that these fibers profoundly modulate the metabolism through the vagal projections in the brain [7]. Chopped waveforms are composed of n stimulating cathodic pulsons of T_{on} duration separated by n-1 non-stimulating pulsons (high impedance phases) of T_{off} duration. The whole of pulsons are followed by an anodic phase to ensure charge balancing. PW_{tot} is defined as the total duration of the cathodic phase whereas PW_{sum} takes into account only the stimulating pulsons within the cathodic phase (Eq. 2). Note that for continuous pulse, $PW_{tot} = PW_{sum} = PW$.

Recently, chopped pulses were investigated in the context of VNS [16] and applied on left cervical vagus nerve of rats. They assessed the ability of chopped rectangular pulses to activate C-fibers and A-fibers compared to a rectangular continuous pulse. Both types of pulses have the same PW_{tot} duration of 200μs. The number of pulsons varied (from 2 to 10), implying different values of T_{on} and T_{off}, that is, different value of PW_{sum}. Their results indicated that by maintaining 50% of C-fibers activated, chopped pulses required 45% less charge than the conventional rectangular pulse and produced 11% less A-fibers activation. They found that rectangular pulse with short duration (40 μs) and chopped rectangular pulse - with short T_{on} (20 μs) and short PW_{sum} (40 μs) - required less charge to maintain the same level of C fibers activation than rectangular pulse with

total duration of 200 μs. Malbert et al. [7] investigated the impact of pulson type stimulation on brain function during chronic VNS applied at the abdominal level on both vagal trunks. They compared one pulson configuration with a more classical single long lasting pulse and found that the pulson configuration was more effective than the single long lasting pulse either for triggering action potential on the afferent vagus or for activation of frontal brain cortices.

Chopped pulses were also investigated in the context of cochlear implant. Shepherd et al. [17] studied the response of single fiber of the auditory nerve, composed of myelinated fibers, to a variety of stimulus waveforms. Among them, biphasic chopped pulses with PW_{sum} of 60 μs were compared to biphasic continuous rectangular pulse with PW duration of 60 μs (with or without interphase gap). Number of pulsons tested was 2, 3 and 6 with respective T_{on} of 30 μs, 20 μs and 10 μs. T_{off} duration were adjusted so that PW_{tot} duration was 120 μs. They found that rectangular continuous pulses with an interphase gap (60 μs) had lower activation thresholds than chopped pulses, whatever the number of pulsons is, and a rectangular pulse without an interphase gap had higher activation threshold (Fig. 8 in [17]).

We recently studied the charge efficiency of chopped pulses were in *lumbricus terrestris* [18] as a simplified model of peripheral nerve. The objective was to evaluate if non-rectangular chopped pulses such as quarter sine and ramp were more charge efficient than rectangular chopped pulse, varying stimulation duration parameters. The results indicated that non rectangular chopped pulses activated Medial Giant Fiber (MGF) and Lateral Giant Fiber (LGF) with less charge than rectangular chopped pulses. For the Medial Giant Fiber MGF (respectively LGF), the gain of charge was up to 33.9% (respectively 17.8%) using chopped ramp, and up to 22.8% (resp. 18.1%) using chopped quarter sine.

The studies of Qing et al., Malbert et al and Shepherd et al. suffer from limitations. They did not compare non-rectangular but continuous waveforms against chopped ones, and the comparison between the efficiency of chopped *versus* continuous waveforms is not straightforward. The main reasons are the interdependence of the stimulus strength and duration (the so-called strength duration curve) and the definition of the duration in order to make a fair comparison, i.e. considering PW_{tot} or PW_{sum}. Indeed the three last studies used PW_{tot} but we hypothesize that a continuous waveform with the same amplitude and PW_{sum} would be more efficient than the chopped one.

In order to better understand the impact of various waveforms on stimulation effectiveness, we have addressed this problem twofolds. We performed experiments in a complex model of the abdominal porcine vagus nerve, and we have completed our study with results of computer simulations. To further concentrate on waveform efficiency we focused on single unit activation instead of a whole nerve activation with recruitment. We thus compared the threshold of activation of a unique fiber against all the tested waveforms.

2. Method

2.1. Chopped pulses

The Fig. 1 shows the waveforms used in experimental studies and modeling. The pulses were biphasic asymmetric and charge-balanced. It consisted of a cathodic phase (continuous or chopped) followed by an anodic phase. The cathodic continuous pulses consisted of a rectangular shape (Fig. 1, **A**), a ramp (Fig. 1, **B**) or a quarter of a sine (quarter sine) (Fig. 1, **C**). The cathodic chopped pulses were composed of multiple pulsons with T_{on} duration. Each pulson was separated by a non-stimulating pulson of T_{off} duration. The chopped pulses shape could be rectangular (Fig. 1, **D**), ramp (Fig. 1, **E**) or quarter sine (Fig. 1, **F**). In order to minimize the influence of anodic phase to avoid misleading interpretations, the charge balancing was performed at low current amplitude and long duration. The anodic phase was identical for all the tested waveforms and consisted of a continuous rectangular pulse of 2.8 ms duration. For all waveforms, the charge at the activation threshold was computed using the formula:

$$Q_{th} = T_{on} \times \sum_{k=1}^{n} I_{th}(k) \qquad (1)$$

Where $I_{th}(k)$ is the current amplitude of pulson k at the activation threshold and n the total number of stimulating pulsons. PW_{sum} is computed as follows:

$$PW_{sum} = \ T_{on} \times n \qquad (2)$$

PW_{tot} is the total duration of the cathodic pulse:

$$PW_{tot} = \ T_{on} \times n + T_{off} \times (n-1) \qquad (3)$$

Note that for the rectangular pulse, $n = 1$ and $T_{on} = PW_{tot} = PW_{sum} = PW$; for the continuous ramp or quarter sine, $PW_{tot} = PW_{sum} = PW$, $T_{off} = 0$.

2.2. Experimental study on porcine model

2.2.1. Ethics statement

A preliminary experiment was performed on one anesthetized female pig to preselect waveforms and to reduce experimental load. The next experiments were carried out on 5 anesthetized female pigs (3 months old, Large White). The experimental procedure was conducted in accordance with the ethical standards of the European and French regulations (Agreements number R-2012-CHM-03 and 00341.01). The experiment consists in stimulating the vagus nerve bilaterally at the level of the thoracic crux while simultaneously recording afferent activity at the the cervical level (left vagus nerve) using the single fiber method [19].

2.2.2. Surgical procedure

Intramuscular injection of ketamine (5 $mg.kg^{-1}$) was used as a pre-anesthesia. Anesthesia was induced by inhalation of isoflurane (5 % v/v). Once anesthetized, pigs were intubated then artificially ventilated and the SpO_2 and $SpCO_2$ were constantly monitored. The first part of the experiment – electrodes implantation on vagus nerves, balloon insertion in the

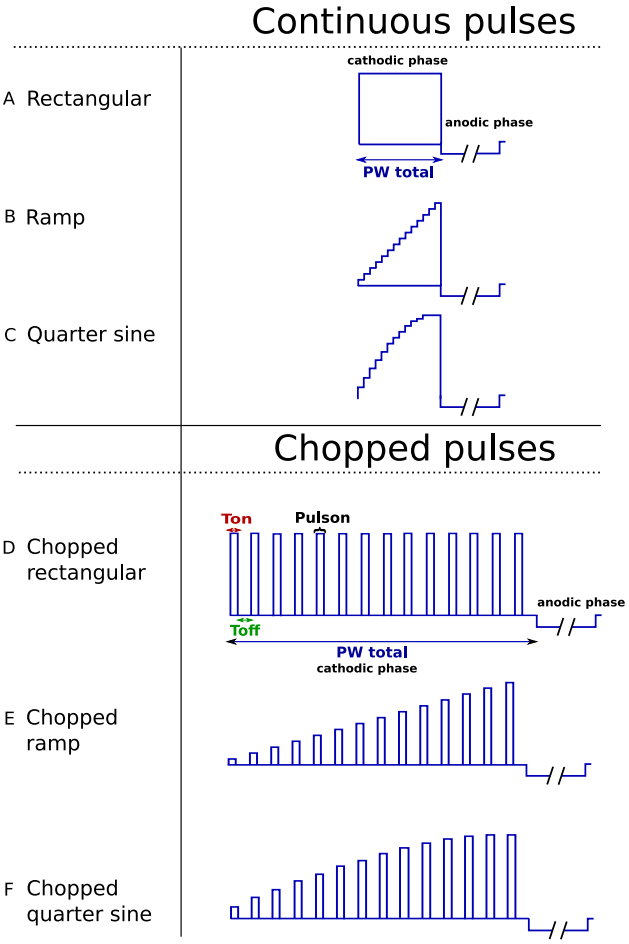

Figure 1: Waveforms used during simulations and experiments. For pig experiments, the anodic phase was always rectangular pulse of 2800 μs duration and amplitude allowing obtaining the same charge as during the cathodic phase.D and E waveforms were tested through simulations.

stomach and left cervical vagus nerve - was done under isoflurane anesthesia. The second part – precise dissection of single fiber, recording and stimulation - was done under pentobarbital anesthesia. In order to inject pentobarbital (20 $mg.kg.hr^{-1}$, Sanofi), a venous cannula was inserted in the ear. Just before recording and until the end of the experiment, D-tubocurarine (0.2 $mg.kg^{-1}$, Sigma) was slowly injected (IV) every 2 hours in order to suppress motion artifacts. Body temperature was maintained at 38.5 $\pm$ 0.5 °C by a self-regulating heating cover placed under the animal. At the end of the experiment, pigs were euthanized by an injection of potassium chloride in the venous cannula in the ear.

2.2.3. Stimulating device implantation

The pig was placed in right lateral decubitus, at the level of the 8th intercostal space an incision was made to reach the mediastinal area. The vagal trunks were isolated as close as possible to the entrance of the diaphragm. Cuff electrodes (Axonic, Sophia Antipolis, France) were placed around the posterior and anterior vagus trunks and maintained by surgical staples placed on the Dacron covered cuffs. The electrodes had a diameter of 3$\pm$0.1 mm. They were made of two rows of two Pt-Ir 10 % contacts (4 in total), short-circuited together to form a bipolar-ring configuration. Surface area of a contact was: 7.56 mm^2 with length of 3 mm and width of 2.52 mm. The distance edge-to-edge between the two rows was 7 mm. The experiment focused on the stimulation and recording of afferent gastric fibers. To be able to verify duodenal origin of the vagus neurons that were recorded, we inserted an inflatable balloon in the stomach of the pig. The insertion of the balloon was achieved while the pig was placed in dorsal decubitus. A midline laparotomy was performed and a balloon

(15 cm long latex balloon with double-lumen catheter ID 3.5 mm for air/retrieval and ID 1.0 mm for pressure sensing) was inserted in the proximal duodenum. The stomach and abdomen were sutured and closed before dissection of the cervical nerve.

2.2.4. Afferent neurons recordings

Stimulation of vagal trunks induced evoked action potentials (APs) which were recorded on the left cervical vagus nerve. Spontaneous and evoked activities of the afferent vagal neurons were recorded using the procedure already described in [19]. Briefly, the skin and cervical muscles surrounding the vagus nerve were attached to a metallic frame creating a pool filled with warmed paraffin oil. The nerve was then microdissected to isolate a bunch of few, possible just one, nerve fibers. The isolated fibers were placed on a recording electrode (tungsten, 50 μm, WPI USA), as shown in Fig. 2. The electrodes were connected to a home-made high impedance differential amplifier (gain 50,000, impedance 20 $M\Omega$) associated with a specifically designed band pass filter (300-6000 Hz). The electroneurogram data (ENG) were digitized at 20 kHz using a custom-made software written under Labview 2011 (National Instruments. USA). Each time a bunch of fibers has been isolated, the balloon in the duodenum was inflated to verify the location of the receptive field of the axon under scrutiny. More precisely, we verified with the ENG whether the distension of the stomach produces APs in those fibers. The inflation procedure was computer controlled to maintain a 20 $mmHg$ pressure within the balloon.

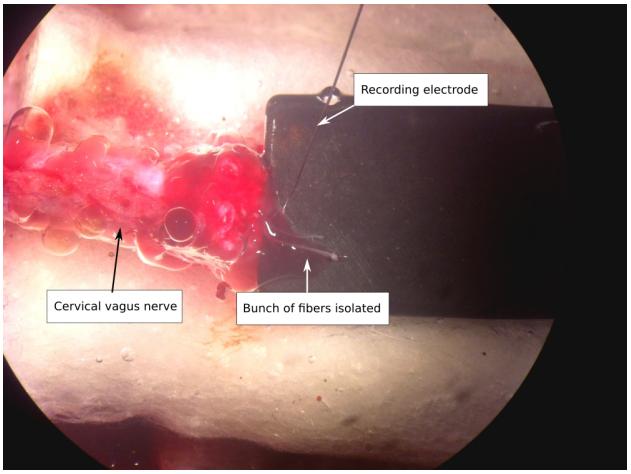

Figure 2: The transected cervical vagus nerve during recordings with the isolated bunch of fibers lying on the of the recording electrode. The diameter of the electrode was 50 μm.

If, during the inflation, we had no evoked AP at the cervical level, we changed the fiber to record until we found a duodenal one. Otherwise, we proceeded with the stimulation protocol.

2.2.5. Stimulation protocol

Stimulation was performed using an external AXIS stimulator (AXONIC, Sophia Antipolis, France). This stimulator is a simplified version of the one described in [20] limited to 4 channels but with higher amplitudes of intensity available (up to 30 mA, 20 V, 10 μA step). Before starting the stimulation protocol, the electrodes' impedance was estimated in order to determine maximal stimulus amplitude that could be delivered without exceeding stimulator's compliance voltage. The used stimulator was designed for humans so the method for impedance estima-

tion is based on [21]: the ratio of the potential drop and the delivered current at the end of 1 ms-long rectangular pulse of 0.5-1 mA amplitude. A stimulation sequencer was build to generate automatically a succession of stimulation patterns of varying shapes and amplitudes. The stimulation protocol was performed for each bunch of vagus gastric fibers found. One vagus nerve (anterior or posterior) was stimulated at a time. The protocol comprised different waveforms with different charges to be tested starting from the lowest to the highest to determine the fiber activation threshold. The initial amplitude for each waveform corresponded to a charge of 1.5 nC. Afterwards, the stimulus amplitude increased exponentially (10% increase rate) and for each amplitude, 6 pulses were generated at a frequency of 2 Hz. There was a pause of 1 s after each series of stimuli. In a preliminary study, all waveforms listed in Fig. 1 were tested, except chopped rectangular, eliminated as a result of experiments reported in [18]. At the outcome of this preliminary study, chopped ramp pulse was eliminated for next studies because few amplitudes could be tested before the maximal stimulus amplitude delivered by the stimulator was reached. For next studies, the protocol comprised 4 waveforms (Fig. 1) with the following characteristics:

- Continuous rectangular pulse, $PW_{tot} = 350\ \mu s$ (Fig. 1, **A**)
- Continuous ramp pulse, $PW_{tot} = 350\mu s$, composed of 14 Ton of 25 μs, no Toff (Fig. 1, **B**)
- Continuous quarter sine pulse , $PW_{tot} = 350\mu s$, composed of 14 Ton of 25 μs , no Toff (Fig. 1, **C**)
- Chopped quarter sine pulse, $PW_{tot} = 1000\mu s$, $PW_{sum} = 350\mu s$ composed of 14 Ton of 25 μs alternated with 13 Toff of 50 μs duration (Fig. 1, **F**)
- Chopped quarter sine pulse, $PW_{tot} = 325\mu s$, $PW_{sum} = 125\ \mu s$ composed of 5 Ton of 25 μs alternated with 4 Toff of 50 μs duration (Fig. 1, **F**)

The rectangular pulse was repeated twice (once at the beginning and once at the end) to check the reliability of the response of the neurons. This procedure was found necessary to assess the stability of the whole protocol from the cell response to the electrode positioning. The trial was rejected if the relative difference between the 2 obtained thresholds were above 10%. The procedure of isolating a bunch of fibers, verifying if they were of duodenal origin, and executing stimulation has been performed during each experiment. The number of iterations strongly depended on the time required to identify the fibers and were limited to the total duration allowed for the experiment i.e. less than 4 hours: the estimated survival time of the vagal afferent neurons once severed from their cell body in the nodose ganglia.

2.3. Data analysis

Evoked APs were processed using Matlab (Mathworks, USA). The recorded ENG were

sorted and counted. For each fiber and waveform, the threshold for activation was determined. We defined a *threshold stability criteria* (TSC) as the minimal amplitude for which AP was evoked for at least 3 out of the 6 stimulus repetitions. When comparing 2 waveforms, n was the number of fibers that passed the *common threshold stability criteria (CTSC)* common to both waveforms and noted: n for $CTSC$. The charge at the activation threshold (Q_{th}) delivered by the stimulator was determined by the formula 1. Statistical analysis was performed on Q_{th} data using R software (R Core Team, Austria). Data were tested for normality with the Shapiro-Wilk test. The comparison of Q_{th} was first performed with a two way repeated measures ANOVA with factors animal and waveforms. Then, Q_{th} obtained with the the different waveforms were compared two by two using the dependent t-test for paired samples, and the Wilcoxon signed rank test in case of non-parametric distribution. Only those pairs of thresholds obtained by two waveforms were analyzed, for which corresponding charge could be delivered during the experiment with both compared waveforms without exceeding the compliance voltage limit. A Bonferroni correction was applied for the multiples tests, the *p-value* presented included this correction. A significance level of 5% was chosen.

2.4. Modeling

2.4.1. Models of nerve and electrode, axon response to stimulation

A volume conductor model for a nerve and cuff electrode coupled with a model of mammalian myelinated nerve fiber was used to study the recruitment mechanisms with the chopped and continuous pulses. The 3D nerve trunk surrounded by a bipolar cuff electrode was modeled using Comsol Multiphysics (COMSOL Inc, Burlington, MA). Modeling of nerve and electrode were previously described in [9, 22]. The nerve model was composed of a fascicle diameter 2.7 mm surrounding the endoneurium. The fascicle was surrounded by a perineurium with a thickness equal to 3% of the fascicle diameter [23] and an epineurium (2.9 mm diameter). A physiological saline layer (50 μm thickness) was modeled between the Cuff electrode and the epineurium. The cuff electrode was modeled according to the same characteristics as described in the experimental section on porcine model (Sec. 2.2.3). A two part process was used to determine fiber activation. The first step was the computing of the step response of the potential fields through the volume conductor model - as a result of electrode stimulation - using COMSOL multiphysics. The second step was to determine the response of a myelinated nerve fiber to the field set up by the cuff electrode system (emission of an AP). Models of mammalian myelinated fibers with 71 Nodes of Ranvier (NoR) were implemented on Matlab (The MathWorks, Natick, Massachusetts). To be consistent with diameter of B-fibers, a 2 μm myelinated axon was modeled, located at 1 mm from the cathode. Two membrane dynamics were used: CRRSS model of a mammalian myelinated fiber at 37°C [24, 25] with perfect insulating myelin, and double cable MRG model [26, 27] at 37°C. The waveforms

were modeled in the same way as the waveforms delivered by the stimulator: continuous quarter sine and the continuous ramp were modeled as n pulsons with identical T_{on} duration without non-stimulating pulsons ($T_{off} = 0\ \mu s$). We thus do not study the influence of the recovery phase and the interstim delay: the anodic phase was not included in simulations. The current threshold amplitude was determined using a dichotomy method. Activation was defined by the induction and propagation of APs along the NoR. Q_{th} was computed using the formula 1.

2.4.2. Waveform study

The modeling study was performed to further extent the results obtained *in-vivo*. All waveforms listed in Fig. 1 were modeled with duration described in Table. 2 and Q_{th} computed. The main objective was to assess which waveforms were more charge-efficient compared to the conventional rectangular pulse. The analyzes were as follows:

- Continuous pulses at $PW = 350\ \mu s$ vs. continuous rectangular at $PW = 350\ \mu s$.
- Chopped pulses at $PW_{sum} = 350\ \mu s$ vs. continuous rectangular at $PW = 350\ \mu s$.
- Chopped pulses at $PW_{tot} = 1000\ \mu s$ vs. continuous rectangular at $PW = 1000\ \mu s$.
- Chopped pulses at $PW_{tot} = 325\ \mu s$ vs. continuous rectangular at $PW = 350\ \mu s$.

Note that $PW_{tot} = 325\ \mu s$ (instead of $PW_{tot} = 350\ \mu s$) for chopped pulse to stay consistent with experiments and technical constraints. The comparison between experimental results and simulations allows to assess the validity of the modeling in such conditions and thus to evaluate the validity of the extension to other waveforms that were not experimentally tested. For all the waveforms, we presented Q_{th} normalized with respect to the charge at the activation threshold of the 350 μs continuous rectangular. A subsidiary question was to evaluate the most relevant duration (i.e. PW_{tot} or PW_{sum}) in order to compare the chopped and the continuous pulses.

3. Results

3.1. Single fiber experiment on the porcine subjects

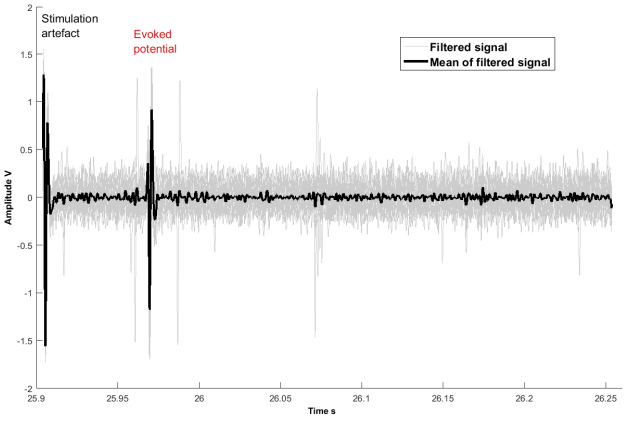

Figure 3: Example of recording of the amplified evoked potential (gain of the amplifier: 50,000). Continuous rectangular pulse with $PW_{tot} = 350\ \mu s$ was used for stimulation.

As described in the method section, we stimulate the nerve distally and recorded dissected single afferent B fibers proximally. A

total of 110 thresholds were determined during 5 experimental sessions. An example of recording, averaged over 6 trials, is shown on the Fig. 3. Stimulation artifact is visible at the beginning of the recording. 36 fibers out of 110 did not pass the TSC regardless of the waveform types. It was possible to distinguish nerve fibers between them owing to the delay between the onset of the stimulation and the evoked AP so the velocity was computed.

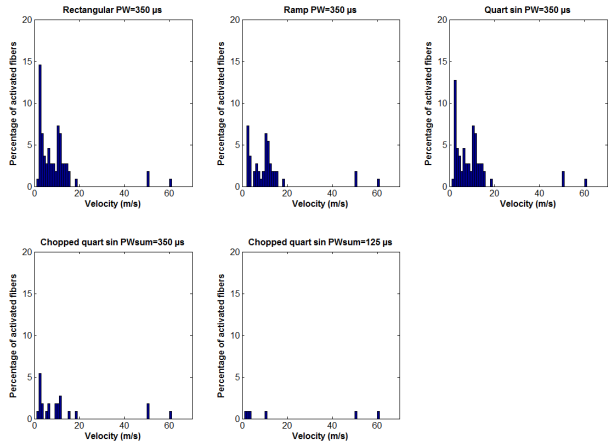

Figure 4: Percentage of gastric nerve fibers activated, as a function of their estimated propagation velocity.

Fig. 4 represents the percentage of fibers that passed TSC as a function of conduction velocity. This percentage was normalized to the total number of fibers recorded (110). Less than 5% of fibers with high velocities (greater than 40 $m.s^{-1}$) were observed. The propagation velocity of these fibers corresponds to type $A\beta$ myelinated neurons. The average propagation velocity of the remaining fibers was 7.54 $m.s^{-1} \pm 4.43m$ $m.s^{-1}$. It allows to identify these fibers to type B and further confirms that afferent gastric fibers includes some B fibers [11].

When testing the influence of factors on Q_{th} ANOVA yielded significant change for both the waveforms type and the animal (two-way repeated measures ANOVA, p-$value$<<0.001). There was no interaction between animal and waveforms (two-way repeated measures ANOVA, p-$value$=0.33). Waveforms were then compared two by two using $CTSC$. Fig. 5 represents Q_{th} at same PW_{sum} for **A**: ramp vs. rectangular, **B**: quarter sine vs. rectangular, **C**: ramp vs. quarter sine, **D**: chopped quarter sine vs. rectangular. In the first step, the ramp and rectangular pulses were compared (Fig. 5, **A**). 49 fibers passed the $CTSC$. Statistical analysis showed that Q_{th} for the ramp pulse was lower than for the rectangular pulse (t-test, p-$value$<<0.01). The mean gain of charge was 485 nC, corresponding to a saving of 19.0% with ramp compared to rectangular. In the second step, quarter sine and rectangular pulses were compared with $n = 68$ for $CTSC$, (Fig. 5, **B**). Results showed that Q_{th} was significantly lower for quarter sine pulse than for the rectangular pulse (Wilcoxon test, p-$value$ << 0.01). The mean charge reduction was 421 nC, corresponding to a saving of 14.5% with quarter sine compared to rectangular. Then, ramp and quarter sine pulses were analyzed with $n = 47$ for $CTSC$ (Fig. 5, **C**). Statistical analysis showed that Q_{th} for the ramp pulse was lower than Q_{th} for the quarter sine pulse (t-test, p-$value$ << 0.01). The mean charge reduction per fibers was 108 nC, corresponding to a saving of 4.2% with ramp compared to quarter

sine. Afterwards, rectangular $PW = 350\ \mu s$ and chopped quarter sine $PW_{tot} = 1000\ \mu s$, $PW_{sum} = 350\ \mu s$ were compared with $n = 23$ for $CTSC$ (Fig. 5, **D**). Comparison was done at PW_{sum}. Statistical analysis showed that Q_{th} for the chopped quarter sine pulse was higher than for the rectangular pulse (t-test, $p\text{-}value << 0.01$). The mean increase was 825 nC, corresponding to an additional consumption of 33.6 % of the chopped quarter sine ($PW_{tot} = 1000\ \mu s$, $PW_{sum} = 350\ \mu s$) compared to the rectangular pulse. Finally, we compared chopped quarter sine $PW_{tot} = 325\ \mu s$, $PW_{sum} = 125\ \mu s$, with rectangular. This time, comparison was done at PW_{tot} with few fibers: $n = 5$ for $CTSC$. The mean charge reduction with chopped quarter sine compared to rectangular was 156 nC (8.8% saving) but there was a doubt on the significance of the results. Indeed, Wilcoxon paired sample test showed a $p\text{-}value$ corrected of 0.1 closed to the threshold of significance of 5%.

In summary, among the waveforms evaluated, the statistical analysis showed that the ramp was the most efficient to activate the duodenal neurons (lowest Q_{th}). Thresholds for quarter sine were close to the ramp (less 5% difference). The rectangular pulse was less efficient than the quarter sine and ramp pulses. At PW_{tot}, The chopped quarter sine pulse was less efficient compared to the rectangular pulse but more efficient if PW_{sum} was used instead.

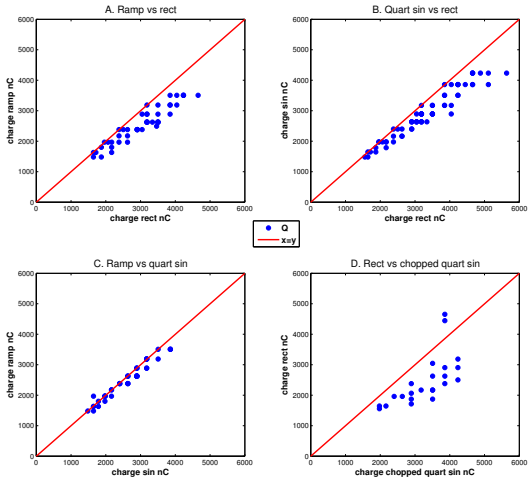

Figure 5: Comparison of Q_{th} between waveforms in the pig experiments. **A**: Ramp $PW = 350\ \mu s$ vs rectangular $PW = 350\ \mu s$, **B**: quarter sine $PW = 350\ \mu s$ vs rectangular $PW = 350\ \mu s$, **C**: Ramp $PW = 350\ \mu s$ vs quarter sine $PW = 350\ \mu s$, **D**: Rectangular $PW = 350\ \mu s$ vs chopped quarter sine $PW_{sum} = 350\ \mu s$, $PW_{tot} = 1000\ \mu s$.

3.2. Modeling

3.2.1. Chopped pulses and continuous pulses

Relative differences of Q_{th} between non-rectangular waveforms and the common continuous rectangular pulse are presented in Table. 1. First, we compared continuous non-rectangular waveforms to the continuous rectangular pulse. The results indicated that Q_{th} was lower for the continuous quarter sine pulse (-23.2%) and the continuous ramp pulse (-30.1%), at the same stimulus duration. These results were qualitatively consistent with the study of Sahin et al. [14]. Second, the chopped waveforms were compared to the continuous rectangular pulse using $PW_{sum} = 350\ \mu s$ (i.e not taking into account the T_{off}). The results indicated that the Q_{th} was significantly higher for the chopped rectangular pulse (+ 128.3%), and

also for the chopped ramp (+ 39.5%) and chopped quarter sine (+ 71.1%). Third, the chopped waveforms were compared to the continuous rectangular pulse using common $PW_{tot} = 350\ \mu s$ (i.e taking into account the T_{off}). Contrary to the previous results, Q_{th} for the chopped rectangular pulse was lower (-18.5%) as well as chopped ramp (-45.8%) and chopped quarter sine (-35.7%). Fourth, the chopped waveforms were compared to the continuous rectangular pulse using common $PW_{tot} = 1000\ \mu s$. The same observation could be drawn than previously: Q_{th} was lower for the chopped rectangular pulse (-20%) as well as chopped ramp (-51.1%) and chopped quarter sine (-40.0%).

3.2.2. Comparison between model and experimental data

The table 2 shows normalized Q_{th} obtained by modeling and porcine experimentation. For the waveforms presented, Q_{th} was normalized with respect to Q_{th} required to activate with the continuous rectangular pulse with $PW = 350\ \mu s$. For the porcine model, the normalized charge was computed for each waveform that passed the $CTSC$ common with continuous rectangular pulse. Quantitatively the results were not comparable, both models used for simulations underestimated the activation thresholds. However, qualitatively, by comparing the chopped and continuous waveforms at the same PW_{sum}, the modeling results corroborated the experimental observations. Indeed, continuous ramp pulse was the most efficient waveform, followed by the continuous quarter sine. Chopped pulses were the least efficient. On the contrary, by comparing waveforms at an equivalent PW_{tot} (Table 2, $PW_{tot} = 325\ \mu s$ and $PW_{tot} = 350\ \mu s$ on the one hand; $PW_{tot} = 1000\ \mu s$ on the other hand) chopped ramp and quarter sine (table 2, PW_{tot} =325) were more efficient than continuous ramp and quarter sine waveforms (table 2, PW_{tot} =350). Concerning the MRG dynamics, the normalized charge for continuous ramp and quarter sine pulses had the same magnitude as those obtained experimentally. The charge decrease was globally underestimated by the CRRSS dynamics. However, for both models, the decrease of charges was overestimated for the quarter sine pulse at $PW_{sum} = 350\mu s$, $PW_{sum} = 1000\mu s$ compared to experimental results.

4. Discussion

4.1. Single fiber experiments on porcine model

Compared to the conventional rectangular pulse with $PW = 350\ \mu s$, the continuous ramp pulse activated duodenal neurons with the lowest charge, followed by the continuous quarter sine pulse and the chopped quarter sine pulse $PW_{sum} = 125\ \mu s$, $PW_{tot} = 325\ \mu s$. The chopped quarter sine $PW_{sum} = 350\ \mu s$, $PW_{tot} = 1000\ \mu s$ was the least efficient among the waveforms. Due to time constraints and technical limitations, only a subset of waveforms have been tested on porcine experiments. Therefore, we skipped those that were known to be less efficient than others (e.g. chopped rectangular, chopped ramp [18]). In our experiments a relatively low number of fibers were activated by

Table 1: Difference of Q_{th} between simulated non-rectangular and rectangular waveforms for $PW = 350\mu s$ and $PW = 1000\mu s$.

Waveform	PW_{sum}	PW_{tot}	Difference relative to the rectangular waveform. (%)	
			Rectangular $PW = 350\ \mu s$	Rectangular $PW = 1000\ \mu s$
Ramp	350	350	-30.1	/
quarter sine	350	350	-23.2	/
Chopped rectangular	350	1000	128.3	-20.0
Chopped ramp	350	1000	39.5	-51.1
Chopped quarter sine	350	1000	71.1	-40.0
Chopped rectangular	125	325	-18.5	/
Chopped ramp	125	325	-45.8	/
Chopped quarter sine	125	325	-35.7	/

chopped waveforms compared to continuous ones (Fig. 4). This was caused by the fact that the chopped waveforms compared to:

1. the corresponding continuous waveforms with the same PW_{tot}, require slightly less charge to activate fibers (table 2), but much higher amplitudes to provide this charge
2. the corresponding continuous waveforms with the same PW_{sum}, require 2 times the same charge to activate the fibers (table 2).

In consequence, in both cases the chopped waveforms were more often exceeding the stimulator compliance voltage before activating the fibers than the corresponding continuous waveforms.

The continuous ramp pulse needs slightly less charge than the continuous quarter sine pulse (4.2%). However, for the same amount of injected charges and the same PW_{sum} the maximum peak currents compared to the rectangular waveform are 2 times higher for a ramp and 1.57 times higher for a quart sine. Since the difference in Q_{th} for those two waveforms is small, and because fewer fibers were activated with ramp compared to quarter sine (Fig. 4), the use of the quarter sine pulse rather than the ramp pulse seems more appropriated in a clinical context.

4.2. Modeling

The modeling study qualitatively confirmed the experimental results on the pig. Moreover, the results normalized to the classical rectangular continuous stimulus, were close between MRG dynamics and experimental data. It indicates that the MRG dynamics is a very appropriate candidate to study non rectangular pulses and in particular multi-pulsons that contains high dynamics, as only a scale factor may be needed to fit experiments and simulations. We thus demonstrated that MRG is able to predict axons' responses to stimulation using chopped

Table 2: Comparison of normalized Q_{th} for chopped and continuous pulses. Units of PW_{tot}, PW_{sum}, T_{on} and T_{off} are μs

Waveform	Porc. exp.	Number of pulsons (T_{on})	PW_{tot}	PW_{sum}	T_{on}	T_{off}	Normalized charge rect 350 μs (%) CRRSS model	Normalized charge rect 350 μs (%) MRG model	Normalized charge rect 350 μs porc. exp. (%)
Rectangular	Yes	1	350	350	350	0	100	100	100
Rectangular	No	1	1000	1000	1000	0	285	205	/
Ramp	Yes	14	350	350	25	0	70	85	84
quarter sine	Yes	14	350	350	25	0	77	88	87
Chopped rectangular	No	14	1000	350	25	50	228	193	/
Chopped ramp	No	14	1000	350	25	50	139	142	/
Chopped quarter sine	Yes	14	1000	350	25	50	171	154	134
Chopped rectangular	No	5	325	125	25	50	82	89	/
Chopped ramp	No	5	325	125	25	50	54	74	/
Chopped quarter sine	Yes	5	325	125	25	50	64	79	91

waveforms whereas MRG's parameters from *in-vivo* were not measured in such conditions. The scale factor mainly comes from the fact that conductivities, extracted from different species and different experimental conditions, and the electrode positioning are not accurate enough. However it can be easily adjusted for a given experimental setup. CRRSS dynamics model is less indicated as results shows much more discrepancies even with a correcting scale factor. These results support the qualitative robustness of the active models, even for stimulation parameters for which they were not designed, i.e., a succession of pulsons on small myelinated fibers. Our study proved that the models can thus be used to virtually investigate a large set of possible waveforms with a high confidence. The only limitation is that the results should be compared against the classic rectangular pulse and not in an absolute manner. Note, however, an exception in the porcine study on chopped quarter sine $PW_{sum} = 125\ \mu s$, $PW_{tot} = 325\ \mu s$, where the models predicted a smaller Q_{th} compared to the continuous ramp and continuous quarter sine pulses. This difference must be mitigated: for the chopped quarter sine $PW_{sum} = 125\ \mu s$, $PW_{tot} = 325\ \mu s$, the number of exploitable samples was small (6 fibers passed the *stability threshold criteria*), and a doubt remained concerning the statistical results. The order of magnitude is respected but the relative values between certain waveforms were so close that it is impossible to experimentally validate this result without a larger set of samples.

4.3. Chopped pulses relevance

The relevance of the comparison between chopped pulses and continuous pulses should be discussed. Indeed, two points of view face in the rare articles on the topic [16], [17]. Should we compare chopped and continuous pulses with the effective stimulation duration (PW_{sum}) or the total stimulation duration (PW_{tot})? The difficulty comes from

the impossibility to uniquely define a stimulation duration, PW, and then an equivalent strength-duration curve. Comparison of chopped and continuous pulses at the same PW_{tot} indicated that the Q_{th} was smaller for the chopped pulses. However, for the same PW_{sum}, i.e. when comparing the chopped waveforms with same continuous waveforms, but without pauses between the pulsons, the continuous waveforms were more efficient. Therefore, we can conclude that the short continuous pulses are the most efficient, this information being already known if we consider the classic strength-duration curves but not obvious when comparing chopped and unchopped waveforms with ambiguous conclusion as reported in previous studies.

Another question is raised by Qing et al. [16]: chopped pulses further discriminate fiber activation by favoring activation of C-fibers and limiting activation of large A-fibers. They associated this observation with the mechanism of prepulses on large diameter fibers. This remark must be mitigated, given that the study by Grill and Mortimer [28] suggested that there is a minimum duration for the prepulses to act on the reduction of excitability (i.e. an increase of the activation threshold). In the study of Grill and Mortimer, prepulses shorter than 200 μs produced an increase in excitability rather than a decrease. Moreover, adding an interpulse between the prepulse and the activation pulse (to be compared with the T_{off} duration) changes the effect on the excitability [29]; this decreases as the duration of the interpulse increases. Instead, we can hypothesize that since the current needed for the activation of the C-fibers is 10 to 100 times greater than the current required to activate A-fibers, it is possible that the large diameter fibers reached their blocking threshold. Indeed, for high current values, virtual anodes [30] can be observed near the cathode, causing an hyperpolarization of the membrane and preventing the AP propagation. Contrary to the previous studies [16], [17], the anodic discharge was identical for all waveforms: a rectangular pulse of 2800 μs. This choice is justified in order to study only the influence of the cathodic phase of stimulation. We thus avoid introducing a confusing factor on the influence of the anodic phase which could distort the comparison between the waveforms. Besides, other consideration such as interpulse after the cathodic phase is not discussed neither studied in this paper and in the cited work on the chopped pulse, but should be considered for further optimization [31, 17]. It becomes very difficult to understand the contribution of each phenomenon to the final result; a great care should be taken when comparing the efficiency of different waveforms as the comparison is based on a non-unique definition of variables, in particular PW. Moreover, the dynamics of the membrane should be related to the timing of the chopped pulse to further understand and then maybe optimized the effect of these intra-pulse high frequency.

5. Conclusion

We have demonstrated in the experimental and modeling studies that it is possible to save charge injection with non-rectangular

waveforms. Results are qualitatively similar between experiments and model prediction further increasing the interest of modeling prior to experimental work. It shows the qualitative robustness of the models even in the case of complex waveforms. The charge reduction depends on waveforms and whether the pulse is chopped or not. The efficiency of chopped waveforms relatively to continuous pulses should be reconsidered based on the way the active pulse duration is computed. However, our study leads to lower the interest of chopped pulse as a continuous waveform with an equivalent PW_{sum}, is always more efficient. Among continuous waveforms, ramp is the most efficient, quarter sine is slightly less efficient and rectangular is much less efficient than those two waveforms. In the pig experiment, for the same current range, continuous quarter sine pulse activates more gastric nerve fibers than ramp waveform, and therefore is an attractive candidate for a long-term use in implanted devices. We showed that chopped pulse mechanisms on axon membrane must be further investigated to make a fair comparison with continuous pulse.

Acknowledgment

MD, PM, CP, and DG drafted the manuscript and all co-authors revised the manuscript. CHM, PM, OR and DG designed the stimulation protocols. CHM designed and performed the surgical approach on porcine subjects. PM and CP acquired and pre-processed experimental data. CP, PM and MD performed statistical analyses. MD and DG defined the numerical implementation of models and algorithms and processed the simulated data. This work was supported by the INTENSE project with a grant from BPI France within the Investments for the Future program in France.

[1] C. DeGiorgio, S. Schachter, A. Handforth, M. Salinsky, J. Thompson, B. Uthman, R. Reed, S. Collin, E. Tecoma, G. Morris, et al., Prospective long-term study of vagus nerve stimulation for the treatment of refractory seizures, Epilepsia 41 (9) (2000) 1195–1200.

[2] G. L. Morris, D. Gloss, J. Buchhalter, K. J. Mack, K. Nickels, C. Harden, Evidence-based guideline update: Vagus nerve stimulation for the treatment of epilepsy report of the guideline development subcommittee of the american academy of neurology, Neurology 81 (16) (2013) 1453–1459.

[3] H. A. Sackeim, A. J. Rush, M. S. George, L. B. Marangell, M. M. Husain, Z. Nahas, C. R. Johnson, S. Seidman, C. Giller, S. Haines, et al., Vagus nerve stimulation (vns^{TM}) for treatment-resistant depression: efficacy, side effects, and predictors of outcome, Neuropsychopharmacology 25 (5) (2001) 713–728.

[4] Z. Nahas, L. B. Marangell, M. M. Husain, A. J. Rush, H. A. Sackeim, S. H. Lisanby, J. M. Martinez, M. S. George,

Two-year outcome of vagus nerve stimulation (vns) for treatment of major depressive episodes., The Journal of clinical psychiatry 66 (9) (2005) 1097–1104.

[5] D. Val-Laillet, A. Biraben, G. Randuineau, C.-H. Malbert, Chronic vagus nerve stimulation decreased weight gain, food consumption and sweet craving in adult obese minipigs, Appetite 55 (2) (2010) 245–252.

[6] D. Guiraud, D. Andreu, S. Bonnet, G. Carrault, P. Couderc, A. Hagège, C. Henry, A. Hernandez, N. Karam, V. Le Rolle, et al., Vagus nerve stimulation: state of the art of stimulation and recording strategies to address autonomic function neuromodulation, Journal of Neural Engineering 13 (4) (2016) 041002.

[7] C.-H. Malbert, E. Bobillier, C. Picq, J.-L. Divoux, D. Guiraud, C. Henry, Effects of chronic abdominal vagal stimulation of small-diameter neurons on brain metabolism and food intake, Brain Stimulation.

[8] C.-H. Malbert, C. Picq, J.-L. Divoux, C. Henry, M. Horowitz, Obesity-associated alterations in glucose metabolism are reversed by chronic bilateral stimulation of the abdominal vagus nerve, Diabetes (2017) db160847.

[9] M. Dali, O. Rossel, D. Andreu, L. Laporte, A. Hernandez, J. Laforet, E. Marijon, A. Hagège, M. Clerc, C. Henry, et al., Model based optimal multipolar stimulation without a priori knowledge of nerve structure: application to vagus nerve stimulation, Journal of neural engineering.

[10] G. Krolczyk, D. Zurowski, J. Sobocki, M. P. Slowiaczek, J. Laskiewicz, A. Matyja, K. Zaraska, W. Zaraska, P. J. Thor, Effects of continuous microchip (MC) vagal neuromodulation on gastrointestinal function in rats, in: Journal of Physiology and Pharmacology, Vol. 52, 2001, pp. 705–715.

[11] N. Mei, M. Condamin, A. Boyer, The composition of the vagus nerve of the cat, Cell and tissue research 209 (3) (1980) 423–431.

[12] M. A. Castoro, P. B. Yoo, J. G. Hincapie, J. J. Hamann, S. B. Ruble, P. D. Wolf, W. M. Grill, Excitation properties of the right cervical vagus nerve in adult dogs., Experimental neurology 227 (1) (2011) 62–8. doi:10.1016/j.expneurol.2010.09.011.

[13] D. R. Merrill, M. Bikson, J. G. Jefferys, Electrical stimulation of excitable tissue: design of efficacious and safe protocols, Journal of Neuroscience Methods 141 (2) (2005) 171–198. doi:10.1016/j.jneumeth.2004.10.020.

[14] M. Sahin, Y. Tie, Non-rectangular waveforms for neural stimulation with practical electrodes., Journal of neural engineering 4 (3) (2007) 227–233.

arXiv:NIHMS150003, doi:10.1088/1741-2560/4/3/008.

[15] S. Jezernik, T. Sinkjaer, M. Morari, Charge and energy minimization in electrical/magnetic stimulation of nervous tissue., Journal of neural engineering 7 (4) (2010) 046004. doi:10.1088/1741-2560/7/4/046004.

[16] K. Y. Qing, M. P. Ward, P. P. Irazoqui, Burst-Modulated Waveforms Optimize Electrical Stimuli for Charge Efficiency and Fiber Selectivity., IEEE transactions on neural systems and rehabilitation engineering : a publication of the IEEE Engineering in Medicine and Biology Society 23 (6) (2015) 936–45. doi:10.1109/TNSRE.2015.2421732.

[17] R. K. Shepherd, E. Javel, Electrical stimulation of the auditory nerve: II. Effect of stimulus waveshape on single fibre response properties., Hearing research 130 (1999) 171–188. doi:Doi 10.1016/S0378-5955(99)00011-8.

[18] M. Dali, O. Rossel, T. Guiho, P. Maciejasz, D. Guiraud, Investigation of the efficiency of the shape of chopped pulses using earthworm model, in: 2018 40th Annual International Conference of the IEEE Engineering in Medicine and Biology Society (EMBC), IEEE. Accepted Manuscript.

[19] G. Cuche, S. Blat, C. H. Malbert, Desensitization of ileal vagal receptors by short-chain fatty acids in pigs., American journal of physiology. Gastrointestinal and liver physiology 280 (5) (2001) G1013–G1021.

[20] D. Andreu, D. Guiraud, G. Souquet, A distributed architecture for activating the peripheral nervous system., Journal of neural engineering 6 (2) (2009) 026001. doi:10.1088/1741-2560/6/2/026001.

[21] D. Guiraud, T. Stieglitz, G. Taroni, J.-L. Divoux, Original electronic design to perform epimysial and neural stimulation in paraplegia, Journal of neural engineering 3 (4) (2006) 276.

[22] M. Dali, O. Rossel, D. Guiraud, Numerical simulation of multipolar configuration and prepulse technique to obtain spatially reverse recruitment order, in: 2016 38th Annual International Conference of the IEEE Engineering in Medicine and Biology Society (EMBC), IEEE, 2016, pp. 5461–5464. doi:10.1109/EMBC.2016.7591962.

[23] Y. Grinberg, M. A. Schiefer, D. J. Tyler, K. J. Gustafson, Fascicular perineurium thickness, size, and position affect model predictions of neural excitation, IEEE transactions on neural systems and rehabilitation engineering 16 (6) (2008) 572–581.

[24] S. Y. Chiu, J. M. Ritchie, R. B. Rogart, D. Stagg, A quantitative description

of membrane currents in rabbit myelinated nerve., The Journal of physiology 292 (1979) 149–66.

[25] J. Sweeney, J. Mortimer, D. Durand, Modeling of mammalian myelinated nerve for functional neuromuscular stimulation., in: IEEE/Engineering in Medicine and Biology Society Annual Conference, IEEE, 1987.

[26] C. C. McIntyre, A. G. Richardson, W. M. Grill, Modeling the excitability of mammalian nerve fibers: influence of afterpotentials on the recovery cycle, Journal of neurophysiology 87 (2) (2002) 995–1006.

[27] C. C. McIntyre, W. M. Grill, D. L. Sherman, N. V. Thakor, Cellular effects of deep brain stimulation: model-based analysis of activation and inhibition, Journal of neurophysiology 91 (4) (2004) 1457–1469.

[28] W. M. Grill, J. T. Mortimer, Inversion of the current-distance relationship by transient depolarization, IEEE Transactions on Biomedical Engineering 44 (1) (1997) 1–9.

[29] C. van den Honert, J. T. Mortimer, The response of the myelinated nerve fiber to short duration biphasic stimulating currents, Annals of biomedical engineering 7 (2) (1979) 117–125.

[30] I. J. Ungar, J. T. Mortimer, J. D. Sweeney, Generation of unidirectionally propagating action potentials using a monopolar electrode cuff, Annals of biomedical engineering 14 (5) (1986) 437–450.

[31] P. Maciejasz, J. Badia, T. Boretius, D. Andreu, T. Stieglitz, W. Jensen, X. Navarro, D. Guiraud, Delaying discharge after the stimulus significantly decreases muscle activation thresholds with small impact on the selectivity: an in vivo study using time, Medical & biological engineering & computing 53 (4) (2015) 371–379.